2012

Isomerization mechanism of the HcRed fluorescent protein chromophore

Qiao Sun
University of Queensland

Zhen Li
University of Wollongong, zhenl@uow.edu.au

Zhenggang Lan
Max Planck Institute of Psychiatry, Munich, Germany

Christoph Pfisterer
University of Heidelberg

Markus Doerr
Max Planck Institute of Psychiatry, Munich, Germany

See next page for additional authors

Publication Details

Sun, Q., Li, Z., Lan, Z., Pfisterer, C., Doerr, M., Fischer, S., Smith, S. C. & Thiel, W. (2012). Isomerization mechanism of the HcRed fluorescent protein chromophore. Physical Chemistry Chemical Physics, 14 (32), 11413-11424.

View Online / Journal Homepage / Table of Contents for this issue
Dynamic Article Links

PCCP

Cite this: *Phys. Chem. Chem. Phys.*, 2012, **14**, 11413–11424

www.rsc.org/pccp

PAPER

Isomerization mechanism of the HcRed fluorescent protein chromophore†

Qiao Sun,*[a] Zhen Li,[b] Zhenggang Lan,[cd] Christoph Pfisterer,[e] Markus Doerr,[cfg] Stefan Fischer,*[e] Sean C. Smith*[ah] and Walter Thiel*[c]

Received 16th April 2012, Accepted 18th June 2012
DOI: 10.1039/c2cp41217a

To understand how the protein achieves fluorescence, the isomerization mechanism of the HcRed chromophore is studied both under vacuum and in the solvated red fluorescent protein. Quantum mechanical (QM) and quantum mechanical/molecular mechanical (QM/MM) methods are applied both for the ground and the first excited state. The photoinduced processes in the chromophore mainly involve torsions around the imidazolinone-bridge bond (τ) and the phenoxy-bridge bond (φ). Under vacuum, the isomerization of the *cis–trans* chromophore essentially proceeds by τ twisting, while the radiationless decay requires φ torsion. By contrast, the isomerization of the *cis–trans* chromophore in HcRed occurs *via* simultaneous τ and φ twisting. The protein environment significantly reduces the barrier of this hula twist motion compared with vacuum. The excited-state isomerization barrier *via* the φ rotation of the *cis*-coplanar conformer in HcRed is computed to be significantly higher than that of the *trans*-non-coplanar conformer. This is consistent with the experimental observation that the *cis*-coplanar-conformation of the chromophore is related to the fluorescent properties of HcRed, while the *trans*-non-planar conformation is weakly fluorescent or non-fluorescent. Our study shows how the protein modifies the isomerization mechanism, notably by interactions involving the nearby residue Ile197, which keeps the chromophore coplanar and blocks the twisting motion that leads to photoinduced radiationless decay.

[a] *Centre for Computational Molecular Science, Australian Institute for Bioengineering and Nanotechnology, The University of Queensland, Qld 4072, Brisbane, Australia. E-mail: q.sun@uq.edu.au*
[b] *Institute for Superconducting & Electronic Materials (ISEM), University of Wollongong, Wollongong, NSW 2500, Australia*
[c] *Max-Planck-Institut für Kohlenforschung, Kaiser-Wilhelm-Platz 1, D-45470 Mülheim an der Ruhr, Germany. E-mail: thiel@mpi-muelheim.mpg.de*
[d] *Qingdao Institute of Bioenergy and Bioprocess Technology, Chinese Academy of Sciences, Qingdao, 266101, P.R. China*
[e] *University of Heidelberg, IWR, D-69120 Heidelberg, Germany. E-mail: stefan.fischer@iwr.uni-heidelberg.de*
[f] *Facultad de Química Ambiental, Universidad Santo Tomás, Carrera 18 No. 9-27, Bucaramanga, Colombia*
[g] *Grupo de Bioquímica Teórica, Escuela de Química, Universidad Industrial de Santander, Carrera 27, Calle 9, Bucaramanga, Colombia*
[h] *Center for Nanophase Materials Sciences, Oak Ridge National Laboratory, Oak Ridge, TN 37831-6496, USA. E-mail: smithsc@ornl.gov*

† Electronic supplementary information (ESI) available: Bond distances in the chromophore model from OM2-MRCI(10,9) and CASSCF calculations[28] as well as deviations between OM2 and CASSCF data; detailed results for the minima and transition states for *cis–trans* isomerization of the chromophore and energy profiles at the SCC-DFTB/MM and B3LYP/MM levels for models A and C of HcRed; videos of molecular movies of the *cis–trans* isomerization of the chromophore under vacuum (*via* τ rotation) and HcRed (*via* HT motion) in the ground state. See DOI: 10.1039/c2cp41217a

Introduction

It is well known that fluorescent proteins (FPs) offer a key advantage as fluorescent probes in that they can be delivered to cells by standard gene transfection methods. In recent years, the green fluorescent proteins (GPPs) and other FPs have become important noninvasive tools for visualization and monitoring of the internal processes within cells or whole organisms, such as protein folding, gene expression, embryogenesis, inflammatory process, protein trafficking, and cell development.[1–10]

Red fluorescent proteins (RFPs) are a subfamily of GFP homologues and possess a chromophore which contains an *N*-acylimine substituent to the *p-hydroxybenzylidine-imidazolinone* (HBI)[11] chromophore functionality of GFPs. The acylimine extends the HBI π electron network and induces a red shift in the absorption and emission relative to GFPs. The absorption and emission wavelengths in the RFPs range from about 550 nm to 600 nm and from about 575 nm to 660 nm, respectively.[12] RFPs have received particular attention, as their emission is well separated from the green-yellow autofluorescence of cells and, moreover, the reduced light scattering at longer wavelengths facilitates imaging of thick tissues. Problems are presented by low quantum yields in the favored

far red/near IR optical window for deep imaging in animal tissue as well as a lesser degree of photostability. Hence, there is a concerted research effort worldwide into engineering improved RFPs with enhanced properties for various types of applications.

HcRed is one of the most red-shifted FPs that have appeared in the literature to date: isolated from *Heteractis crisp* with an emission maximum at 645 nm.[13] The crystal structure of HcRed has been determined to 2.1 Å resolution.[13] Chromophores within the GFP-like family can adopt long-lived alternative conformations despite sharing similar chromophore sequences. For example, the chromophore (Met63-Tyr64-Gly65) in the highly far-red fluorescent protein eqFP611 is in a *trans*-coplanar conformation,[14] and *trans–cis* isomerization leads to a red shift of the fluorescence.[15] The chromophore (Gln66-Tyr67-Gly68) in the non-fluorescent chromoprotein Rtms5 has a *trans*-non-coplanar conformation,[16] whereas the same chromophore sequence in the highly fluorescent DsRed shows a *cis*-coplanar conformation.[17] In our HcRed protomers, the cyclic tripeptide chromophore (Glu64-Tyr65-Gly66) can adopt both *cis*-coplanar and *trans*-non-coplanar conformations indicating some mobility within the protein cavity. Simulated annealing omit maps reveal that the *cis*-coplanar conformation of the tyrosyl moiety gives the best match of the recorded electron density. The available experimental data suggest that the *cis*-coplanar conformation is responsible for the bright fluorescent properties of HcRed,[13] while the *trans*-non-coplanar conformation is associated with the weak or non-fluorescence of hcCP, the chromoprotein parent of HcRed. Interestingly, *cis–trans* isomerization of chromophores has recently also been recognized as a key feature of the mechanism of kindling of certain chromoproteins.[18,19] The *cis–trans* photoisomerization of the chromophore in fluorescent proteins shows a behavior of ON/OFF switching. The interest for photo-switchable fluorescent proteins lies in their potential as fluorescent labels, selectively addressable by optical means.

Rational development of improved RFPs depends on a solid base of knowledge of the chemical physics of the chromophore functionality, which should in principle allow us to understand how interactions within the protein influence fluorescence color and quantum yield. Theoretical studies can provide selective and detailed insight into structure, mechanism and function of RFPs that is otherwise not easily obtained. Density functional theory (DFT) as well as complete-active-space self-consistent-field (CASSCF) methods have been used to study the chromophore either bare under vacuum or clustered under vacuum with small-molecule mimics of neighboring amino acid residues that are present in the protein. This work has helped establish some mechanistic principles relating largely to the intrinsic properties of the chromophore (*e.g.* see ref. 13, 20–31). Although quantum mechanical/molecular mechanical (QM/MM) methods have been developed considerably over the past decade (for recent reviews see ref. 32, 33), it remains challenging to perform accurate calculations with explicit inclusion of the surrounding solvated protein matrix environment. In the QM/MM approach, the "active center" and the environment are computed using an appropriate quantum mechanical method and a classical force field, respectively. This hybrid method enables a robust QM-based approach to the simulation of complex systems,[32,33] for example catalytic reactions of cytochrome P450 enzymes,[34,35] NMR chemical shifts of vanadium-dependent chloroperoxidase,[36] solvent effects on the electronic adsorption spectrum of guanine,[37] and photoactive yellow protein.[38] Our groups have previously studied the structural and energetic properties as well as the absorption spectra of some RFPs (DsRed.M1 and HcRed).[39–42]

In recent years, there has been much progress in theoretical research on electronically excited states, with MS-CASPT2 (multi-state complete-active-space second-order perturbation theory)[43,44] and coupled cluster methods (CC2, CCSD, CC3)[45–47] being well established for small molecules. Moreover, time-dependent density functional theory (TD-DFT)[48] has become popular for calculations on medium-sized molecules, giving reasonable results for various (but not all) types of excited states at relatively low computational cost.[49] The reliable description of electronically excited states in large biological systems, such as FPs, is however still very challenging. Accurate *ab initio* methods such as MS-CASPT2 and CC3 are restricted to small molecules, and the computational cost for simpler treatments such as CC2 still rises steeply with molecular size. TD-DFT is an attractive choice because of its computational efficiency and the availability of analytical gradients, but there are a number of well-documented problems of TD-DFT,[49] for example, with regard to charge-transfer states[50] and singlet or triplet instabilities.[51]

In light of this, we have chosen the orthogonalization-corrected OM2 semiempirical Hamiltonian[52,53] and the GUGA-CI approach[54] as implemented in the MNDO program[55] to study the isomerization mechanism of the chromophore under vacuum and in HcRed. Our choice of using mainly OM2-MRCI for the excited-state calculations in this study is based on the following considerations. Firstly, the orthogonalization-corrected OM*x* methods are better suited than the standard semiempirical methods (MNDO, AM1, PM3) for treating excited states, since they include additional terms in the Fock matrix that represent Pauli exchange repulsions in an approximate manner. These terms effectively raise the energy of antibonding virtual MOs and of the associated excited states. Therefore, one would expect an improved performance the OM*x* methods not only for ground-state properties, but also for excited-state properties, even though the latter had not been taken into account during the OM*x* parametrization. Secondly, there have been a number of successful OM2-MRCI applications published so far that support this view. These include studies on the electronically excited states of the retinal and rhodopsin chromophore,[56,57] a careful validation for the vertical excitation energies in a benchmark set of 28 organic chromophores,[58] and excited-state surface-hopping dynamics simulations at the QM and QM/MM level for several small molecules, such as nucleobases, azobenzenes, fluorene-based molecular rotary motors, and a modified GFP chromophore.[59–66]

We begin below by considering the RFP chromophore under vacuum. The minimum energy pathway (MEP) for *cis–trans* isomerization of the bare chromophore in the ground electronic state was examined by geometry optimizations at the SCC-DFTB and B3LYP/TVZP levels as well as single-point

B3LYP calculations at SCC-DFTB optimized structures. We present OM2-MRCI results for equilibrium geometries and energetic properties of the chromophore model in its ground and first excited states as well as for the relevant conical intersections. We discuss the isomerization reactions of the isolated RFP chromophore before moving on to calculations for the chromophore in HcRed. We report the MEPs for torsional isomerization of the chromophore in the native protein at the SCC-DFTB/MM level, followed by single-point calculations at the DFT(B3LYP/TVZP)/MM level. Finally, we present the OM2-MRCI/MM results for the isomerization pathways in the ground and the first excited state, and we discuss the *trans–cis* isomerization mechanism as well as the mechanism of radiationless decay of *cis*- and *cis–trans* conformations of the chromophore in HcRed. Based on the computational results for the RFP chromophore model under vacuum and in the solvated HcRed protein, we are able to gain insight into the mechanism of the isomerization reactions and explain why the chromophore is non-fluorescent under vacuum, and why the *cis*-coplanar conformation of the chromophore is fluorescent in HcRed while the *trans*-non-planar one is weakly fluorescent or non-fluorescent. Furthermore, we also show that the protein environment, especially the residue Ile197, has a very significant effect on the fluorescent properties of HcRed, which we believe provides very useful contextual information to guide mutation studies directed toward improved RFPs.

Methodology

Ground state simulations

In the ground-state calculations on the bare chromophore model, designated R_0 (see Fig. 1 and for more details ref. 28), the MEP was studied at three different levels of theory: geometry optimizations with the SCC-DFTB method as implemented in CHARMM[67] and with B3LYP/TZVP using Gaussians03,[68] and single-point calculations at the B3LYP/TZVP//SCC-DFTB level.

Concerning the ground-state calculations on HcRed, we previously found that different protonation states of the titratable active-site residues Glu214 and Glu146 critically influence the manner in which the relative stability and the degree of planarity of the *cis*- and *trans*-conformers vary with pH.[41] Thus, three models with different protonation states of Glu146 and Glu214 around the chromophore were used. According to the calculated pK_a values, in model B under neutral conditions (pH = 7), Glu146 should be deprotonated and Glu214 should be protonated. In model A both Glu214 and Glu146 are protonated (acidic conditions), and in model C both Glu214 and Glu146 are deprotonated (basic conditions).[41]

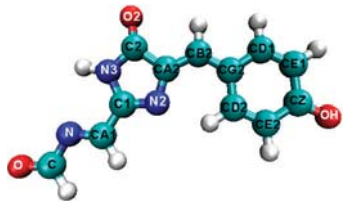

Fig. 1 Numbering scheme for the chromophore model (R_0).

The MEPs for isomerization of the *cis–trans* conformer of the chromophore in HcRed were determined by using the Conjugate Peak Refinement (CPR) algorithm[69] as implemented in the TReK module of CHARMM. The MEP calculation started from an initial guess of the path, which was built here by combined interpolation in Cartesian and internal coordinates[70] of the *cis–trans* isomerization reaction pathway, allowing 3000 protein atoms in HcRed to move freely (see below). This method has been used previously to determine the mechanisms of several complex reactions in proteins, such as proton transfer in bacteriorhodopsin and GFP, as well as the mechanism of the recovery stroke in the Myosin molecular motor.[71–73]

Four snapshots, serving as initial structures for QM/MM optimization, were taken at 100 ps intervals from the 500 ps MD trajectories of the *cis*-chromophore in HcRed.[41] For the QM/MM geometry optimizations, only part of the total system was optimized while the remaining atoms were frozen at the snapshot geometry. The optimized active region in HcRed was defined using a distance criterion, whereby any residue that contains an atom within 20 Å of any atom of the chromophore is included. The same active region was used for the *cis–trans* isomerization of the chromophore in HcRed. The QM region was treated with the Self-Consistent-Charge Density Functional Tight Binding (SCC-DFTB) method.[74] Please see ref. 41 for the detailed information on the QM region. The QM/MM boundary was described by the generalized hybrid orbital (GHO) method. The energy for the MM region was calculated using the CHARMM force field with the all-atom parameter set 22.[75] The single-point energies of the *cis*- and *trans*-chromophore and their transition states were calculated at the DFT/MM level, with the B3LYP functional[76,77] and the TZVP basis set,[78] at SCC-DFTB/MM optimized structures. The TURBOMOLE program[79] was used for the QM treatment in the DFT/MM calculations. The MM part of the system was represented by the CHARMM force field as implemented in the DL_POLY program.[80] The QM/MM calculations were performed with the ChemShell package[81,82] that integrates the TURBOMOLE or MNDO and DL_POLY programs.

The total energy of the full QM/MM system includes the energy of the QM subsystem (E_{QM}), the energy of the MM subsystem (E_{MM}), and the interaction energy between QM and MM subsystems (electrostatic, van der Waals, and bonded interactions). In practice, the electrostatic interaction between the QM and MM subsystems is included in the QM calculation through the addition of MM point charges to the QM Hamiltonian, whereas the bonding and van der Waals (vdW) interactions between the QM and MM subsystems are determined in the MM calculation. Thus, the total energy can be expressed as:

$$E_{total} = E_{(QM,MM)} + E_{(MM,QM)} \quad (1)$$

where $E_{(QM,MM)}$ is the sum of E_{QM} and the electrostatic interaction energy between the QM and MM subsystems, and $E_{(MM,QM)}$ is the sum of E_{MM} and the vdW and bonded interactions between the MM and QM subsystems.

Excited state simulations

For the excited-state calculations, the semiempirical MNDO program was used for the QM treatment in the QM and

QM/MM calculations.[55] The orthogonalization-corrected OM2 semiempirical Hamiltonian[52,53] and the GUGA-CI approach[54] were employed to compute the required energies, gradients, and nonadiabatic coupling vectors. Geometry optimizations of energy minima and conical intersections were performed with the DL-FIND optimizer in Chemshell using the limited-memory Broyden–Fletcher–Goldfarb–Shanno and Lagrange–Newton algorithms, respectively.[83–85] In the multi-reference configuration interaction (MRCI) treatment, three reference configurations were used (closed-shell, single, and double HOMO–LUMO excitations). Four different active spaces (m,n) were tested with m electrons in n molecular orbitals (MOs): (10, 9), (12, 11), (12, 12), and (14, 13), which include 5, 6, 6, and 7 occupied π MOs, and 4, 5, 6, and 6 unoccupied π* MOs, respectively, from the conjugated π system. The π system of the chromophore is the same as in the chromophore model in ref. 28. To always retain the π orbitals in the active space, we used a recently developed method for identifying and tracking the π character of orbitals (applying a threshold of 0.4 for the sum of the local π populations).[86] In these tests, the calculated excitation energies did not change significantly upon increasing the size of the active space (see below). Hence, the smallest active space (10, 9) was chosen as standard for the OM2-MRCI excited-state calculations, both under vacuum and in HcRed.

To investigate the effect of interactions between the chromophore and the protein environment in HcRed, we examined coordinate-driving representations of the pathways characterized by the torsions τ and φ (see below). Potential energy surface (PES) scans were generated by fixing one (or both) of the two bridge dihedrals (the driving coordinates) in the chromophore and minimizing all other degrees of freedom subject to this constraint. The first driving coordinate, the dihedral angle τ between the sites N2_CA2_CB2_CG2 (Fig. 1), represents progress along a path τ that leads to photoisomerization of the imidazolinone-bridge bond. The second one, the dihedral angle φ between the sites CA2_CB2_CG2_CD1 (Fig. 1), describes the rotation around the phenoxy-bridge bond. The results of these PES scans allow us to see which types of motions are most strongly modified when going from the bare chromophore to the protein-embedded chromophore.

Four snapshots of the *cis*-conformer of the chromophore in HcRed were optimized at the OM2-MRCI/MM level to determine the emission energies. For the energy profile of the hula twist (HT) motion in the excited state, τ and φ were fixed at the values found in the ground state MEP calculations. For identifying the transformation of the *cis* and *trans* isomers of the chromophore in HcRed, the PES scans were generated by fixing φ and minimizing the other degrees of freedom in the active region; to save computational effort, this was done only for snapshot 1, since the torsional behavior in the ground state had been found to be similar in all four snapshots considered.

Results and discussions

We begin by considering the bare chromophore, both from the perspective of validating our methods and providing insights by comparisons with the subsequent QM/MM calculations that include the whole protein.

RFP chromophore model under vacuum

Fig. 1 and 2 show the numbering scheme adopted for the atomic sites in the chromophore model (R_0) and the four isomerization pathways considered for the chromophore. Table 1 lists the relevant dihedral angles and relative energies of the optimized *cis*, *trans* and transition state (*TS*) structures resulting from the ground-state calculations. The SCC-DFTB and B3LYP/TZVP results are in good agreement with each other.

Structural and energetic properties of the bare chromophore at the OM2-MRCI level

We now focus on the minima and conical intersections of the chromophore model under vacuum, both in the ground and the first excited singlet state. In Table S1 of the ESI†, the optimized bond lengths from OM2-MRCI and CASSCF calculations[28] are listed as well as the deviations between OM2-MRCI and CASSCF data: the corresponding root mean square deviation (RMSD) is 0.039 Å. Table 2 presents the two key torsion angles τ and φ. OM2-MRCI and CASSCF yield identical values for the minima in the ground and first excited singlet state

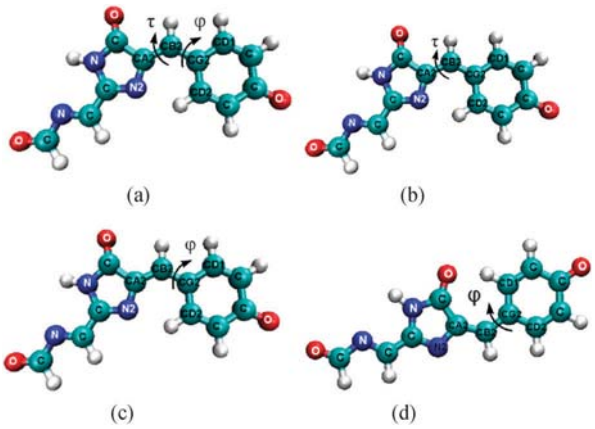

Fig. 2 The four isomerization pathways of the chromophore under vacuum: (a) *cis*–*trans* isomerization by simultaneous φ and τ rotation (hula twist motion); (b) *cis*–*trans* isomerization by τ rotation; (c) φ rotation in the *cis* isomer; and (d) φ rotation *in the trans* isomer. Because of symmetry, (c) and (d) are identity transformations (see text).

Table 1 Relative energies (kcal mol^{-1}) and dihedral angles (°) of *cis*, *trans* and transition state (TS) structures of the ground-state RFP chromophore under vacuum

		SCC-DFTB	B3LYP/TZVP	B3LYP/TZVP// SCC-DFTB
Dihedral angles				
cis	τ	0.0	0.0	[a]
	φ	0.0	0.0	[a]
TS	τ	93.8	92.7	[a]
	φ	3.8	0.5	[a]
trans	τ	180.0	180.0	[a]
	φ	0.0	0.0	[a]
Relative energies				
Cis		0.0	0.0	0.0
TS-τ		22.3	19.4	19.2
trans		1.4	2.0	1.84

[a] Same as for SCC-DFTB.

Table 2 Dihedral angles in minima and conical intersections of the RFP chromophore model at the OM2-MRCI(10,9) level. *Ab initio* CASSCF results from ref. 28 are given for comparison

Species	Dihedral angle (°)	OM2-MRCI(10,9)	CASSCF[28]
cis-S_0-min(R_0)	τ	0.0	0.0
	φ	0.0	0.0
cis-S_1-plan	τ	0.0	0.0
	φ	0.0	0.0
trans-S_0-min	τ	180.0	180.0
	φ	0.0	0.0
trans-S_1-plan	τ	180.0	180.0
	φ	0.0	0.0
S_1-τ	τ	90.2	82.6
	φ	4.2	7.4
trans-S_{01}-φ	τ	180.0	180.0
	φ	92.3	91.9
cis-S_{01}-φ	τ	0.0	0.0
	φ	90.8	90.7
S_{01}-τ	τ	94.2	100.8
	φ	9.3	31.9

(labeled *cis*-S_0-min(R_0), *trans*-S_0-min, *cis*-S_1-plan, and *trans*-S_1-plan), which are planar in all cases (0 or 180°). For the conical intersections related to φ torsion (*cis*-S_{01}-φ and *trans*-S_{01}-φ), the differences in the optimized φ values are tiny (0.4° and 0.1°, respectively). For the structures involving τ twisting (*trans–cis* isomerization: minimum in the first excited state S_1-τ and conical intersection S_{01}-τ), the differences between the OM2-MRCI and CASSCF results are somewhat larger (7.6° and 6.6° for τ; 3.2° and 22.6° for φ). Overall, the agreement between the optimized OM2-MRCI and CASSCF structures can be considered satisfactory, even in the case of the conical intersections.

Table 3 lists the adiabatic and vertical energies of the minima and conical intersections obtained from OM2-MRCI calculations with four different active spaces: (10, 9), (12, 11), (12, 12), and (14, 13). It is obvious that increasing the active space from (10, 9) to (14, 13) does not influence these energy values too much. Hence, the smallest active space (10, 9) was adopted for all further excited-state OM2 calculations.

Next we compare the energies from OM2-MRCI(10,9) calculations with published *ab initio* results.[28] In the ground state of the chromophore, the *cis*-conformation (*cis*-S_0-min) is slightly more stable than the *trans*-conformation (*trans*-S_0-min) by 0.03 eV (OM2-MRCI) and 0.10 eV (CASSCF and MRPT2). The vertical excitation energies for the *cis*- and *trans*-conformers obtained from OM2-MRCI (2.17 and 2.28 eV) are in good agreement with those from MRPT2 (2.20 and 2.35 eV), while CASSCF gives higher values as expected (2.69 and 2.91 eV). At the optimized planar excited-state geometries (*cis*-S_1-plan and *trans*-S_1-plan), the energy differences to the ground state are again similar for OM2-MRCI (1.70 and 1.75 eV) and for MSPT2 (1.76 and 1.91 eV), but larger for CASSCF (2.14 and 2.09 eV). Although there is a relatively big difference between the OM2-MRCI (1.63 eV) and MRPT2 (0.99 eV) methods of the adiabatic energy for the perpendicular excited-state minimum (S_1-τ) in the ground state, the energy of S_1-τ relative to the ground state is also similar in OM2-MRCI (2.57 eV) and MSPT2 (2.49 eV), with the CASSCF value again being higher (2.99 eV). For the three conical intersections (bottom three entries in Table 3), we can only compare with the less reliable CASSCF data since MSPT2 values are not available; as expected, OM2-MRCI predicts these conical intersections to occur at lower energies than in CASSCF. Overall, the OM2 method appears to provide a reliable and reasonably accurate description of the energetic properties of the relevant minima and conical intersections in the RFP chromophore.

Isomerization pathways of the bare chromophore model

We have examined the MEP for ground-state *cis–trans* isomerization of the bare chromophore at different levels of theory (as summarized in the Methodology section). The barrier for *cis–trans* isomerization is computed as 22.3, 19.4 and 19.2 kcal mol^{-1} using SCC-DFTB, B3LYP/TZVP, and B3LYP/TZVP//SCC-DFTB (Table 1). At the transition state, the B3LYP/TZVP optimized torsional angles τ and φ are 92.7° and 0.5° (Table 1), indicating that the *cis–trans* isomerization for the bare ground-state chromophore model proceeds *via* a twist of the dihedral angle τ. This will be contrasted below with the mechanism of isomerization in the HcRed protein.

Table 3 Adiabatic and vertical energies (eV) of energy minima and conical intersections from OM2-MRCI calculations with different active spaces. *Ab initio* MSPT2 and CASPT2 results from ref. 28 are given for comparison

		Adiabatic energies						Vertical energies					
Method		OM2				MRPT2	CASSCF	OM2				MRPT2	CASSCF
Active space		(10,9)	(12,11)	(12,12)	(14,13)		(12,11)	(10,9)	(12,11)	(12,12)	(14,13)		(12,11)
cis-S_0-min(R_0)	S_0	0.00	0.00	0.00	0.00	0.00	0.00						
	S_1	2.17	2.19	2.15	2.11	2.20	2.69	2.17	2.19	2.15	2.11	2.20	2.69
cis-S_1-plan	S_0	0.25	0.29	0.26	0.31	0.22	0.42						
	S_1	1.95	1.94	1.91	2.00	1.98	2.55	1.70	1.65	1.65	1.69	1.76	2.14
trans-S_0-min	S_0	0.03	0.03	0.02	0.03	0.10	0.10						
	S_1	2.31	2.33	2.29	2.25	2.45	3.01	2.28	2.30	2.27	2.22	2.35	2.91
trans-S_1-plan	S_0	0.31	0.35	0.32	0.31	0.33	0.56						
	S_1	2.06	2.05	2.01	2.00	2.24	2.64	1.75	1.70	1.70	1.69	1.91	2.09
S_1-τ	S_0	1.63	1.52	1.56	1.68	0.99	1.27						
	S_1	2.57	2.48	2.55	2.67	2.49	2.99	0.95	0.96	0.99	0.99	1.50	1.72
trans-S_{01}-φ	S_0/S_1	1.74	1.89	1.98	1.98		2.12						
	S_2	3.55	3.68	3.79	3.79								
cis-S_{01}-φ	S_0/S_1	1.56	1.61	1.69	1.87		1.99						
	S_2	3.48	3.47	3.55	3.72								
S_{01}-τ	S_0/S_1	2.46	2.71	2.72	2.72		4.05						
	S_2	4.97	5.22	5.14	5.14								

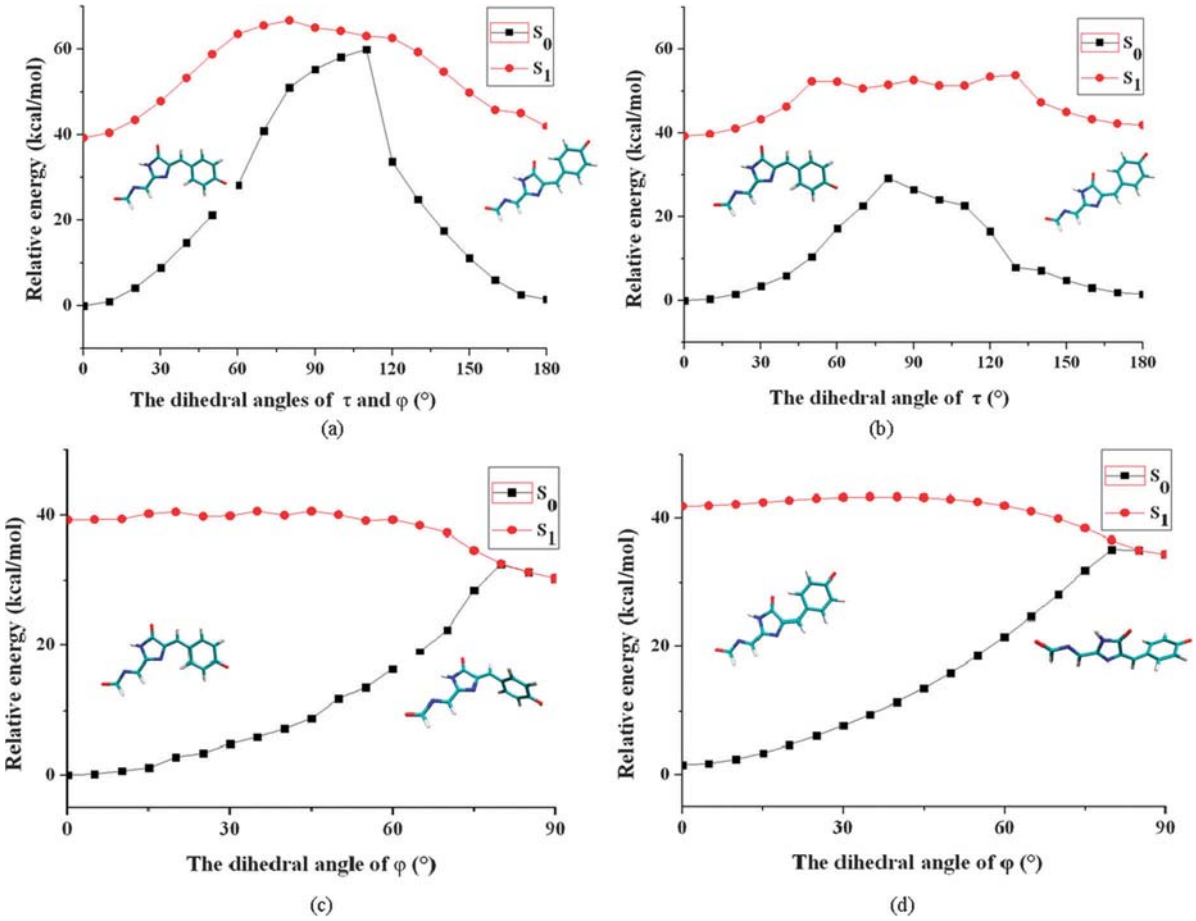

Fig. 3 OM2-MRCI energy profiles of the four isomerization pathways defined in Fig. 2, for the bare chromophore under vacuum (see text).

To examine the excited-state energetics of different types of twisting motions in the bare chromophore, we have computed profiles along different pathways defined by driving coordinates (Fig. 2). These PES scans were performed at the OM2-MRCI level for the first excited singlet state followed by single-point ground-state calculations. Fig. 3 shows the resulting OM2-MRCI energy profiles for the four pathways explored: (a) the hula twist (HT) motion involving simultaneous rotation around the φ and τ dihedral angles; (b) the double-bond isomerization by rotation around τ; (c) the identity transformation in the *cis* isomer through rotation of 180° about φ; (d) the corresponding identity transformation in the *trans* isomer. The coplanar geometries at $\varphi = 0°$ (or 180°) and $\tau = 0°$ (*cis* isomer) or 180° (*trans* isomer) are true energy minima for the bare chromophore.

The OM2-MRCI energy profiles of the RFP chromophore confirm that the *cis–trans* isomerization *via* the twist of the bridge dihedral τ is feasible, with barriers of 29.2 and 14.5 kcal mol^{-1} for the S_0 and S_1 state, respectively (Fig. 3). The ground-state barrier is somewhat higher than the fully optimized values of 19–22 kcal mol^{-1} for B3LYP/TZVP and SCC-DFTB (Table 1). The barriers of *cis–trans* isomerization *via* HT motion involving simultaneous changes in the two bridge dihedrals τ and φ are quite high, with values of 59.9 and 27.4 kcal mol^{-1} in the S_0 and S_1 state, respectively. The identity transformation *via* φ rotation (phenoxy-bridge angle) is found to be almost barrierless in the excited state for both the *cis*- and *trans*-conformers. Obviously, in the first excited singlet state, path τ is strongly disfavored compared to path φ. This results in a tendency to twist the phenoxy-bridge bond in the excited state at small τ values of the imidazolinone-bridge torsion, leading to a curve crossing event with likely radiationless decay to the ground state. We have previously studied this kind of radiationless decay of the bare RFP chromophore *via* a twisted intermolecular charge-transfer state.[28] Here, we focus on the alternative isomerization mechanism *via* HT motion, the barrier of which may be smaller or even completely disappear in specific protein environments. In the following, we present our QM/MM results for the *cis–trans* isomerization of the chromophore in HcRed and analyze the environmental effects on the mechanism.

Isomerization of the chromophore in HcRed

MEPs for *cis–trans* isomerization in HcRed in the ground state

Compared with τ rotation, the HT motion sweeps out a smaller volume and should thus be favored if the chromophore is constrained within a tight protein cavity. Hence, for the fully solvated HcRed protein, we only address the HT mechanism for *cis–trans* isomerization.[87] As in our previous work,[41] we consider three models of HcRed that differ in the protonation

Table 4 Relative energies (kcal mol^{-1}) of *cis* and *trans* conformers and of the transition states of HcRed (ground state, model B) from SCC-DFTB/MM optimizations and from DFT(B3LYP/TZVP)/MM single-point calculations for snapshots 1–4

Snapshot	*cis*	TS	*trans*
SCC-DFTB/MM			
1	0.0	53.9	9.1
2	0.0	52.0	6.5
3	0.0	51.9	4.9
4	0.0	46.7	8.8
B3LYP/MM// SCC-DFTB/MM			
1	0.0	64.5	11.7
2	0.0	60.4	8.3
3	0.0	59.9	6.3
4	0.0	55.7	10.6

states of Glu residues near the anionic chromophore (A: Glu214 and Glu146 both protonated; B: Glu214 protonated and Glu146 deprotonated; C: Glu214 and Glu146 both deprotonated).

Table 4 lists the relative energies for the *cis*- and *trans*-conformers and the associated transition state for model B of HcRed obtained from SCC-DFTB/MM geometry optimizations and single-point DFT(B3LYP/TZVP)/MM//SCC-DFTB/MM calculations. Results are given for four snapshots taken from the SCC-DFTB/MM dynamical simulations. A detailed breakdown into QM energies and MM contributions is provided in the ESI† (Table S3).

Fig. 4 shows the optimized *cis*-, *trans*-, and TS structures of the HcRed chromophore for snapshot 1. The structural information such as important dihedral angles and hydrogen bond distances of *cis* and *trans* conformers and the transition state of HcRed are listed in Table S2 in ESI.† Fig. 5a depicts the variation in the dihedral angles τ and φ along the computed MEPs, while the relative SCC-DFTB/MM energies along the isomerization pathways are plotted in Fig. 5b for the four snapshots of HcRed.

For HcRed model B (most appropriate for ambient pH), the computed energies (Table 4) always favor the *cis*- over the *trans*-conformers, by 4.9–9.1 kcal mol^{-1}, which is consistent with the experimental observation and previous computational results.[13,41] Analogous data for models A and C, as well as the contributions of $E_{(QM,MM)}$ and $E_{(MM,QM)}$, are given in the ESI† (Tables S4–S7). In model C (most appropriate for high pH), the *cis*-form is again more stable, by 8.7–15.4 kcal mol^{-1}. By contrast, the stability order is inverted in the case of model A (most appropriate for low pH): here, the relative energies of the *trans*-conformer lie between −0.5 and −5.1 kcal mol^{-1}, which implies that the chromophore will preferentially adopt the

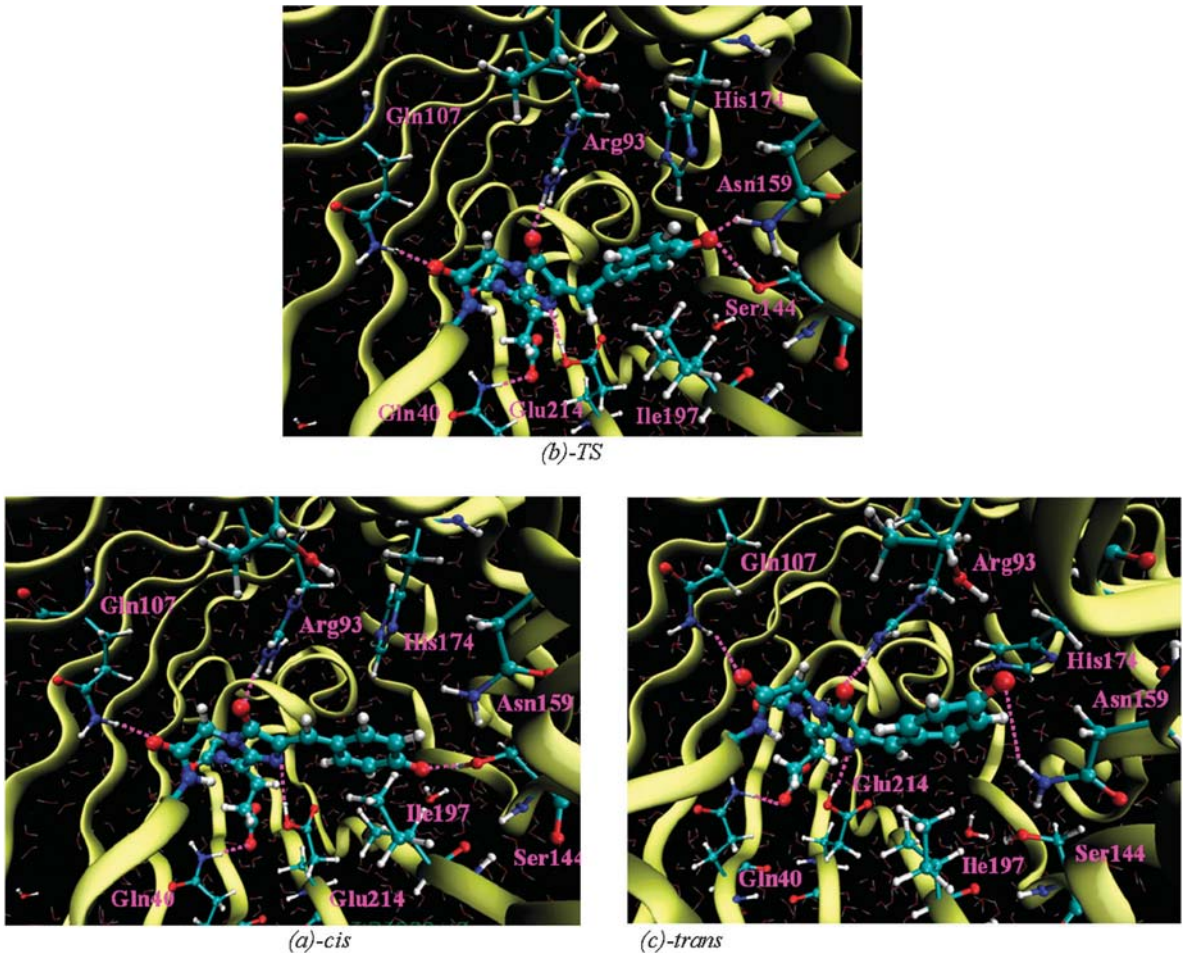

Fig. 4 Optimized SCC-DFTB/MM structures for snapshot 1 of the chromophore of HcRed in the ground state: (a) *cis*-conformer, (b) transition state (TS), (c) *trans*-conformer.

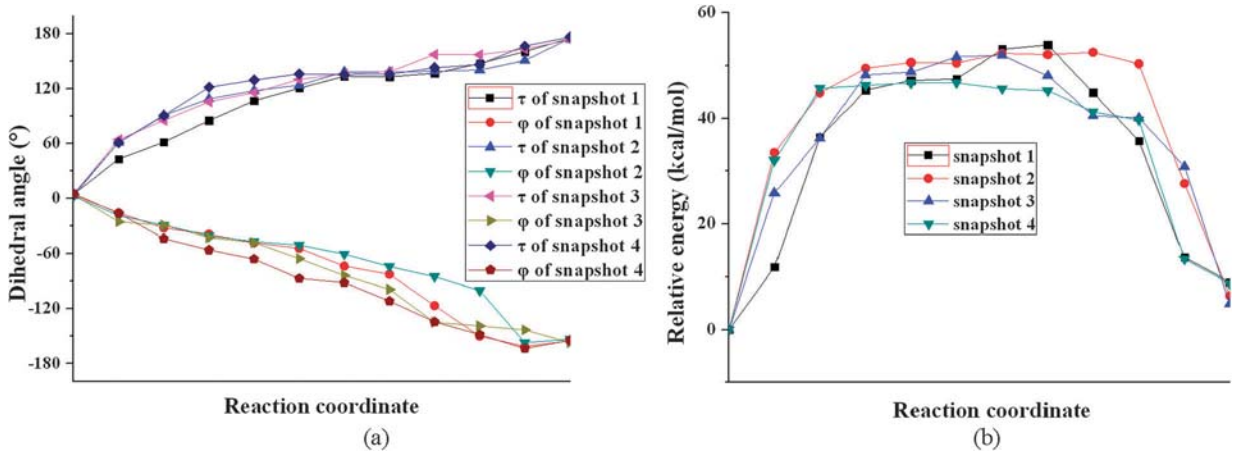

Fig. 5 (a) Dihedral angles and (b) relative energies along the *cis–trans* isomerization pathway of the chromophore of HcRed in the ground state for snapshots 1–4, calculated at the SCC-DFTB/MM level.

trans-conformation in model A. The SCC-DFTB results for different protonation states thus indicate that the titratable active-site residues Glu214 and Glu146 can critically influence the manner in which the relative stability of the *cis*- and *trans*-conformers varies with pH, which is in line with our previous study.[41]

For model B, the SCC-DFTB/MM barriers for *cis–trans* isomerization in the ground state of the four snapshots are 53.9, 52.0, 51.9, and 46.7 kcal mol^{-1}, respectively. Single-point DFT(B3LYP/TVZP)/MM calculations at the SCC-DFTB/MM structures yield barriers of 64.5, 60.4, 59.9, and 55.7 kcal mol^{-1}, respectively. For model C, the computed barriers to *cis–trans* isomerization range between 44.8 and 64.9 kcal mol^{-1}, while in model A with the inverted stability order, the corresponding barriers lie between 39.1 and 47.5 kcal mol^{-1} at these computational levels. All these calculated ground-state barriers are quite high, implying that the two alternative *cis*- and *trans*-conformers are "frozen" in their positions during the process of maturation in HcRed and should not be able to equilibrate under ambient conditions – at least insofar as ground-state dynamics is concerned.

Isomerization of the chromophore in HcRed in the S_1 state

One snapshot of model B with protonated Glu214 and deprotonated Glu146 nearby the chromophore of HcRed has been chosen for the excited state calculations.[41] Fig. S1 in ESI† shows the optimized OM2-MRCI/MM geometries of excited-state minima and S_{01} conical intersections of the chromophore in HcRed: (a) the *cis*-chromophore in the S_1 state; (b) the conical intersection for *cis–trans* isomerization *via* HT motion; and the conical intersections reached *via* φ rotation from (c) the *cis*-isomer and (d) the *trans*-isomer. Tables 5 and 6 list the relevant dihedral angles and adiabatic energies. The optimized structures of the conical intersections (c) and (d) in HcRed are obviously quite similar to those under vacuum (see Tables 2 and 5). They are characterized by an out-of-plane displacement of the phenoxy ring, which is almost perpendicular to the imidazolinone ring, with dihedral angles φ and φ* ranging from 86.2 to 94.8°. For the conical intersection of *cis–trans* isomerization *via* HT motion, there is a moderate out-of-plane displacement of the CB2 and HB atoms in the bridge (Fig. 1) and a small pyramidalization of the bridge atoms of the two rings, CA2 and CG2, with an improper dihedral angle CA2_CB2_CG2_HB of 152.7°. The CB2–HB bond is almost perpendicular to the phenoxy ring (with values −82.0 and 113.0° for φ and φ*, respectively), and the CB2–HB bond deviates significantly from the plane of the imidazolinone ring (with values 133.0 and −53.0° for τ and τ*, respectively).

Table 7 lists the calculated emission energies and oscillator strengths of the *cis*-isomer of the chromophore in HcRed. The emission energies for the four snapshots are computed to be 2.06, 2.19, 2.08 and 2.11 eV, in good agreement with the experimental emission maximum at 1.92 eV (645 nm).[13] It has not been possible to locate the S_1 minimum of the *trans*-isomer in HcRed by geometry optimizations starting from the available S_0 minima, because all optimizations ended up at *trans*-S_{01}-φ conical intersections. The reason could be that

Table 5 Dihedral angles in the minima and conical intersections of the RFP chromophore in HcRed obtained at the OM2-MRCI/MM level

Species	τ	τ*	φ	φ*
cis-S_0	11.2	−161.7	1.2	179.3
cis-S_1	−4.4	−170.8	21.6	−159.1
cis-S_{01}-φ	17.3	−160.3	−86.2	89.7
trans-S_0	175.6	17.9	−158.0	23.1
trans-S_{01}-φ	164.7	−8.1	−94.8	87.4
S_{01}-HT	133.0	−53.0	−82.0	113.0

τ* and φ* are the dihedral angles of C2_CA2_CB2_CG2 and CA2_CB2_CG2_CD1, respectively (see Fig. 1).

Table 6 Adiabatic energies (eV) of energy minima and conical intersections of the RFP chromophore in HcRed computed at the OM2-MRCI/MM level

Species	S_0_$E_{(QM,MM)}$	S_1_$E_{(QM,MM)}$	$E_{(MM,QM)}$	S_0_E_{total}	S_1_E_{total}
cis-S_0	0.00	2.91	0.00	0.00	2.91
cis-S_1	0.64	2.70	−0.12	0.53	2.59
cis-S_{01}-φ	1.92	1.92	0.38	2.30	2.30
trans-S_0	0.10	3.06	0.44	0.54	3.49
trans-S_{01}-φ	1.44	1.44	0.66	2.10	2.10
S_{01}-HT	2.82	2.82	−0.07	2.75	2.75

Table 7 Emission energies (eV) and oscillator strengths f of the *cis*-conformer of the chromophore of HcRed from OM2-MRCI/MM and Exp. value (eV)

	OM2-MRCI(10,9)/MM		Exp.[13]
Snapshot	Emission energy (eV)	f	(eV)
1	2.06	0.66	1.92
2	2.19	0.71	
3	2.08	0.69	
4	2.11	0.71	

trans-isomer of the chromophore in HcRed is non-planar in the ground state: the dihedral angle φ is 48.2° experimentally,[13] and our computed value is 22.0°. The *cis*-isomer of the chromophore in HcRed is co-planar in the ground state, and the computed dihedral angle φ is 1.2°. In the conical intersections of *trans*-S_{01}-φ and *cis*-S_{01}-φ, the phenoxy rings are almost perpendicular to the imidazolinone rings. We can see that the Franck–Condon structure generated by vertical excitation of *trans* conformation is closer to the structure of *trans*-S_{01}-φ conical intersection than that of the *cis* one.

The isomerization mechanisms of the chromophore in HcRed protonation model B (snapshot 1) have been studied in detail with the OM2-MRCI/MM method. Fig. 6a shows the energy profiles obtained for the *cis–trans* isomerization of the chromophore in HcRed *via* the HT motion in the ground state and the first excited singlet state, with plots of the QM ($E_{(QM,MM)}$) energies, the MM energies ($E_{(MM,QM)}$) and the total energies (E_{total}), see eqn (1). Starting from the structures determined *via* CPR in the ground state, the OM2-MRCI/MM energy profiles for *cis–trans* isomerization in the S_1 state were calculated with the two crucial torsion angles fixed at the ground-state MEP values, while relaxing the other degrees of freedom in the active region. In the ground state, the $\Delta E_{(QM,MM)}$, $\Delta E_{(MM,QM)}$ and ΔE_{total} values for *cis–trans* isomerization in HcRed *via* HT motion are computed (OM2-MRCI/MM) to be 59.8, −0.2, and 59.6 kcal mol^{-1}, respectively, in rather good agreement with those from DFT/MM. In the first excited singlet state, the corresponding $\Delta E_{(QM,MM)}$, $\Delta E_{(MM,QM)}$ and ΔE_{total} values are 23.0, −4.9, and 18.1 kcal mol^{-1}, respectively; intriguingly, for the reverse *trans–cis* isomerization, the values are 12.9, −6.6 and 6.3 kcal mol^{-1}, respectively, and thus much lower than those for the chromophore under vacuum (with a barrier ΔE_{total} around 27 kcal mol^{-1}). This can be traced back to differences in hydrogen bonding along the pathway between the *cis*- and the *trans*-isomer, in particular to hydrogen bonds formed by the phenoxy oxygen atom. Two hydrogen bonds involving Ser144 and a water molecule in the *cis*-conformation (see Fig. 4a) are replaced by two hydrogen bonds formed with Ser144 and Asn159 at the transition state (see Fig. 4b) and one hydrogen bond formed with Asn159 in the *trans*-conformation (Fig. 4c), implying an energy penalty for the *trans*-isomer. This weakening of hydrogen bonding interactions for the *trans*-isomer in comparison with the *cis*-isomer implies a lower barrier on the S_1 surface for the *trans*-form on the route to accessing the conical intersection and thereby undergoing isomerization and radiationless decay to the ground state. Thus, our calculations imply that an excited-state isomerization in HcRed *via* HT motion is much more feasible than that of the chromophore model under vacuum or indeed that of HcRed in the ground electronic state.

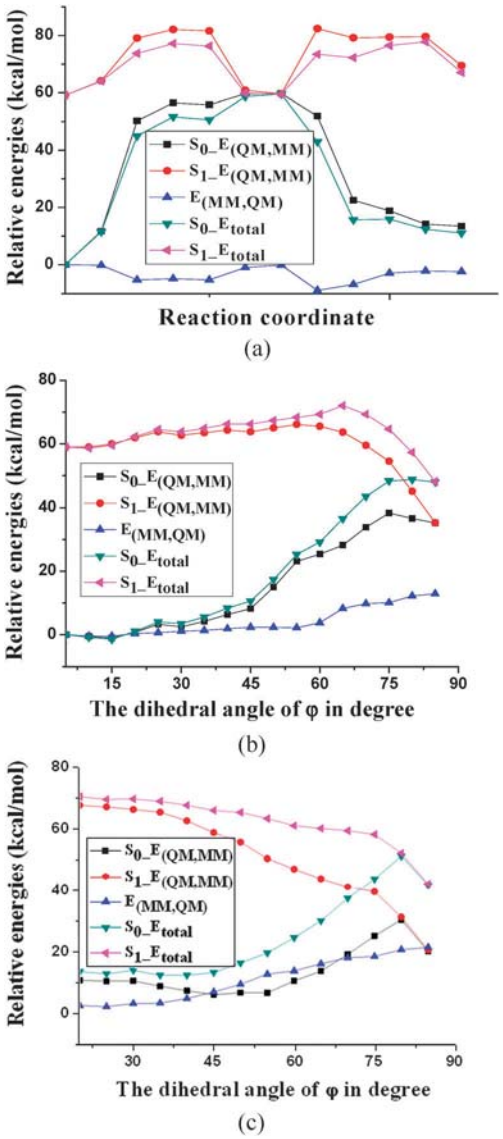

Fig. 6 OM2-MRCI/MM energy profiles for the chromophore of HcRed in the S_0 and S_1 state: (a) *cis–trans* isomerization *via* HT motion; (b) φ rotation in the *cis*-isomer; and (c) φ rotation in the *trans*-isomer.

Fig. 6b and c show analogous energy profiles for φ rotation in the *cis*- and *trans*-conformations of the chromophore in HcRed, respectively. Recall (Fig. 3) the finding for the bare chromophore that these two excited-state pathways (involving only twisting around the phenoxy-bridge bond of the chromophore) lead to conical intersections virtually without any barrier, indicating that radiationless decay to the ground state will be the likely outcome after photoexcitation. For the chromophore in HcRed, the reaction profiles in Fig. 6b and c show the energies of the conical intersections to be lower again than those of the *cis* and *trans* S_1 minima, respectively. However, contrary to the case of the bare chromophore, there is a sizable barrier in HcRed for the *cis*-isomer in the S_1 state on the way toward the intersection, which amounts

to 13.0 kcal mol^{-1} (with $\Delta E_{(QM,MM)}$ and $\Delta E_{(MM,QM)}$ contributions of 4.7 and 8.3 kcal mol^{-1}). For the *trans*-non-coplanar form there is no such barrier (Fig. 6c). This implies that the *cis*-conformer of the chromophore in the excited state should have a longer lifetime before accessing the intersection and undergoing radionless decay compared with the *trans*-conformer. A noteworthy structural feature that likely contributes to this effect is the hydrophobic amino acid Ile197 nearby the *cis*-conformation of chromophore. The two methyl groups of Ile197 are parallel to the phenoxy ring of the chromophore and will thus tend to keep the *cis*-chromophore coplanar and to block the isomerization reaction of *cis*-coplanar-conformation *via* φ or τ rotation. Clearly, subtle structural interactions within the chromophore cavity of the protein environment have a significant effect on the fluorescence properties of the chromophore in HcRed. By characterizing transition states and energy profiles for isomerization along the various possible pathways, our study provides for the first time qualitative answers for the questions as to why the chromophore is non-fluorescent under vacuum and why the *cis*-coplanar conformation of the chromophore in HcRed is fluorescent, while the *trans*-non-coplanar conformation is weakly fluorescent or non-fluorescent.

Conclusions

The isomerization mechanism of an RFP chromophore in the ground state and the first excited singlet state has been explored under vacuum and in the HcRed protein using a range of QM and QM/MM methods.

For the RFP chromophore under vacuum, the relevant minimum structures and conical intersections have been optimized at the OM2-MRCI level. The comparison of the computed structural and energetic properties with those from CASSCF and MRPT2 calculations indicates that OM2-MRCI is a reliable and robust method for this system. The *cis–trans* isomerization *via* τ twisting is found to be feasible, with barriers of 29.2 and 14.5 kcal mol^{-1} in the S_0 and S_1 state, respectively. The barriers to *cis–trans* isomerization *via* hula twist motion, involving simultaneous τ and φ rotation, are significantly higher, with values of 59.9 and 27.4 kcal mol^{-1}, respectively. The identity transformations by φ torsion are barrierless in the S_1 state, indicating that the photoinduced radiationless decay of the *cis*- and *trans*-chromophore under vacuum occurs *via* this mechanism.

For the RFP chromophore in HcRed with protonation model B (most appropriate for ambient pH), the *cis–trans* isomerization mechanism in the ground state has been studied at the SCC-DFTB/MM and DFT (B3LYP/TZVP)/MM levels. Reaction barriers between the non-fluorescent (*trans*) and fluorescent (*cis*) forms – determined from relaxed MEPs computed from snapshots taken along the ground-state dynamical simulations – are in the range of 37.9–52.8 kcal mol^{-1}, while barriers for the reverse reaction (*cis–trans*) are in the range of 46.7–64.5 kcal mol^{-1} at these two levels. For models A and C with different protonation states of Glu214 and Glu146 close to the chromophore, the barriers for the *cis–trans* isomerization are also very high. These results indicate that the two alternate conformations of the chromophore in HcRed should be "frozen" in their respective positions during the process of maturation and – insofar as can be inferred from the ground-state dynamics at least – may not be in equilibrium in the mature protein.

The various possible isomerization mechanisms of the chromophore in model B HcRed (snapshot 1) were calculated using the OM2-MRCI/MM method. Starting from the ground-state structures of HcRed obtained from the CPR path optimization, we computed the energy profiles of *cis–trans* isomerization with the two crucial torsion angles fixed while relaxing other degrees of freedom in the active region. In the ground state, the barrier of *cis–trans* isomerization *via* the HT motion is 59.6 kcal mol^{-1}, while that for the reverse reaction (*trans–cis*) is 48.6 kcal mol^{-1}, in good agreement with the DFT/MM results. In the first excited singlet state, the barrier for the *cis–trans* isomerization in HcRed is 18.1 kcal mol^{-1} (*trans–cis*: 6.3 kcal mol^{-1}). Obviously, the excited-state *trans–cis* isomerization of the chromophore in HcRed *via* the HT motion is much easier than the corresponding process under vacuum (activation: 6.3 *vs.* 24.4 kcal mol^{-1}), which implies that the protein environment significantly lowers the barrier of this photoinduced isomerization reaction. The interactions between the chromophore in its *trans*-non-coplanar conformation and the nearby residues Asn159 and Ser144 stabilize the chromophore, and especially the conical intersection of *cis–trans* isomerization *via* HT motion. For the excited-state isomerization *via* φ rotation, the barrier of the *cis*-coplanar conformer of the chromophore in HcRed (13.0 kcal mol^{-1}) is computed to be higher than that of the *trans*-non-coplanar form (no barrier). The protein environment thus has a significant influence on the fluorescent properties of HcRed, especially through residue Ile197 (with its two methyl groups positioned parallel to the phenoxy part of the nearby chromophore), which keeps the *cis*-conformation of the chromophore coplanar and blocks the photoinduced reactions involving an isomerization by rotation along the φ and τ modes.

By studying the possible isomerization mechanisms of the chromophore under vacuum and in the protein, our study answers the question why the chromophore is non-fluorescent under vacuum and why the *cis*-coplanar-conformation of chromophore is related to the fluorescent properties in HcRed, while the *trans*-non-planar conformation is weakly fluorescent or non-fluorescent.

Acknowledgements

Qiao Sun gratefully acknowledges the support by a Queensland International Fellowship and Australian Research Council Discovery Project DP1095906. Zhen Li thanks for the support from a Queensland Smart Future Fellowship and a Queensland International Fellowship. We acknowledge the computing resources from the University of Queensland (namely, the Computational Molecular Science cluster computing facility), the Australian National Computational Infrastructure (NCI), the Max-Planck-Institut für Kohlenforschung, Mülheim, and the University of Heidelberg, IWR, Germany. We also acknowledge useful discussions with Elsa Sanchez-Garcia and Seth Olsen.

Notes and references

1 R. Y. Tsien, *Annu. Rev. Biochem.*, 1998, **67**, 509.
2 V. V. Verkhusha and K. A. Lukyanov, *Nat. Biotechnol.*, 2004, **22**, 289.
3 Y. J. Passamaneck, A. Di Gregorio, V. E. Papaioannou and A. K. Hadjantonakis, *Microsc. Res. Tech.*, 2006, **69**, 160.
4 D. M. Chudakov, S. Lukyanov and K. A. Lukyanov, *Trends Biotechnol.*, 2005, **23**, 605.
5 C. N. Stewart, *Trends Biotechnol.*, 2006, **24**, 155.
6 D. Shcherbo, E. M. Merzlyak, T. V. Chepurnykh, A. F. Fradkov, G. V. Ermakova, E. A. Solovieva, K. A. Lukyanov, E. A. Bogdanova, A. G. Zaraisky, S. Lukyanov and D. M. Chudakov, *Nat. Methods*, 2007, **4**, 741.
7 S. A. Wacker, F. Oswald, J. Wiedenmann and W. Knochel, *Dev. Dyn.*, 2007, **236**, 473.
8 G. Seitz, S. W. Warmann, J. Fuchs, U. A. Mau-Holzmann, P. Ruck, H. Heitmann, R. M. Hoffman, J. Mahrt, G. A. Muller and J. T. Wessels, *J. Pediatr. Surg.*, 2006, **41**, 1369.
9 R. M. Hoffman, *Curr. Top. Dev. Biol.*, 2005, **70**, 121.
10 R. M. Hoffman, *J. Biomed. Opt.*, 2005, **10**, 041202.
11 L. A. Gross, G. S. Baird, R. C. Hoffman, K. K. Baldridge and R. Y. Tsien, *Proc. Natl. Acad. Sci. U. S. A.*, 2000, **97**, 11990.
12 Y. A. Labas, N. G. Gurskaya, Y. G. Yanushevich, A. F. Fradkov, K. A. Lukyanov, S. A. Lukyanov and M. V. Matz, *Proc. Natl. Acad. Sci. U. S. A.*, 2002, **99**, 4256.
13 P. G. Wilmann, J. Petersen, A. Pettikiriarachchi, A. M. Buckle, S. C. Smith, S. Olsen, M. A. Perugini, R. J. Devenish, M. Prescott and J. Rossjohn, *J. Mol. Biol.*, 2005, **349**, 223.
14 J. Petersen, P. G. Wilmann, T. Beddoe, A. J. Oakley, R. J. Devenish, M. Prescott and J. Rossjohn, *J. Biol. Chem.*, 2003, **278**, 44626.
15 K. Nienhaus, H. Nar, R. Heilker, J. Wiedenmann and G. U. Nienhaus, *J. Am. Chem. Soc.*, 2008, **130**, 12578.
16 M. Prescott, M. Ling, T. Beddoe, A. J. Oakley, S. Dove, O. Hoegh-Guldberg, R. J. Devenish and J. Rossjohn, *Structure*, 2003, **11**, 275.
17 M. A. Wall, M. Socolich and R. Ranganathan, *Nat. Struct. Biol.*, 2000, **7**, 1133.
18 D. M. Chudakov, A. V. Feofanov, N. N. Mudriku, S. Lukyanov and K. A. Lukyanov, *J. Biol. Chem.*, 2003, **278**, 7215.
19 J. M. Battad, P. G. Wilmann, S. Olsen, E. Byres, S. C. Smith, S. G. Dove, K. N. Turcic, R. J. Devenish, J. Rossjohn and M. Prescott, *J. Mol. Biol.*, 2007, **368**, 998.
20 S. Olsen, M. Prescott, P. Wilmann, J. Battad, J. Rossjohn and S. C. Smith, *Chem. Phys. Lett.*, 2006, **420**, 507.
21 S. F. Wang and S. C. Smith, *J. Phys. Chem. B*, 2006, **110**, 5084.
22 H. Zhang, S. F. Wang, Q. Sun and S. C. Smith, *Phys. Chem. Chem. Phys.*, 2009, **11**, 8422.
23 R. B. Zhang, M. T. Nguyen and A. Ceulemans, *Chem. Phys. Lett.*, 2005, **404**, 250.
24 P. Altoe, F. Bernardi, M. Garavelli, G. Orlandi and F. Negri, *J. Am. Chem. Soc.*, 2005, **127**, 3952.
25 Y. Y. Ma, Q. A. Sun, H. Zhang, L. A. Peng, J. G. Yu and S. C. Smith, *J. Phys. Chem. B*, 2010, **114**, 9698.
26 S. Olsen, K. Lamothe and T. J. Martinez, *J. Am. Chem. Soc.*, 2010, **132**, 1192.
27 S. Olsen and R. H. McKenzie, *J. Chem. Phys.*, 2009, **130**, 184302.
28 S. Olsen and S. C. Smith, *J. Am. Chem. Soc.*, 2007, **129**, 2054.
29 S. Olsen and S. C. Smith, *J. Am. Chem. Soc.*, 2008, **130**, 8677.
30 O. Vendrell, R. Gelabert, M. Moreno and J. M. Lluch, *J. Am. Chem. Soc.*, 2006, **128**, 3564.
31 O. Vendrell, R. Gelabert, M. Moreno and J. M. Lluch, *J. Phys. Chem. B*, 2008, **112**, 5500.
32 H. M. Senn and W. Thiel, *Top. Curr. Chem.*, 2007, **268**, 173.
33 H. M. Senn and W. Thiel, *Angew. Chem., Int. Ed.*, 2009, **48**, 1198.
34 S. Shaik, S. Cohen, Y. Wang, H. Chen, D. Kumar and W. Thiel, *Chem. Rev.*, 2010, **110**, 949.
35 S. Shaik, D. Kumar, S. P. de Visser, A. Altun and W. Thiel, *Chem. Rev.*, 2005, **105**, 2279.
36 M. P. Waller, M. Buhl, K. R. Geethalakshmi, D. Q. Wang and W. Thiel, *Chem.–Eur. J.*, 2007, **13**, 4723.
37 M. Parac, M. Doerr, C. M. Marian and W. Thiel, *J. Comput. Chem.*, 2010, **31**, 90.
38 G. Groenhof, M. Bouxin-Cademartory, B. Hess, S. P. de Visser, H. J. C. Berendsen, M. Olivucci, A. E. Mark and M. A. Robb, *J. Am. Chem. Soc.*, 2004, **126**, 4228.
39 E. Sanchez-Garcia, M. Doerr, Y.-W. Hsiao and W. Thiel, *J. Phys. Chem. B*, 2009, **113**, 16622.
40 E. Sanchez-Garcia, M. Doerr and W. Thiel, *J. Comput. Chem.*, 2010, **31**, 1603.
41 Q. Sun, M. Doerr, Z. Li, S. C. Smith and W. Thiel, *Phys. Chem. Chem. Phys.*, 2010, **12**, 2450.
42 Y.-W. Hsiao, E. Sanchez-Garcia, M. Doerr and W. Thiel, *J. Phys. Chem. B*, 2010, **114**, 15413.
43 K. Andersson, P. A. Malmqvist and B. O. Roos, *J. Chem. Phys.*, 1992, **96**, 1218.
44 K. Andersson, P. A. Malmqvist, B. O. Roos, A. J. Sadlej and K. Wolinski, *J. Phys. Chem.*, 1990, **94**, 5483.
45 O. Christiansen, H. Koch and P. Jorgensen, *Chem. Phys. Lett.*, 1995, **243**, 409.
46 O. Christiansen, H. Koch and P. Jorgensen, *J. Chem. Phys.*, 1995, **103**, 7429.
47 E. V. Gromov, I. Burghardt, H. Köppel and L. S. Cederbaum, *J. Phys. Chem. A*, 2011, **115**, 9237.
48 E. Runge and E. K. U. Gross, *Phys. Rev. Lett.*, 1984, **52**, 997.
49 A. Dreuw and M. Head-Gordon, *Chem. Rev.*, 2005, **105**, 4009.
50 A. Dreuw and M. Head-Gordon, *J. Am. Chem. Soc.*, 2004, **126**, 4007.
51 F. Cordova, L. J. Doriol, A. Ipatov, M. E. Casidaa, C. Filippi and A. Vela, *J. Chem. Phys.*, 2007, **127**, 164111.
52 W. Weber, *PhD thesis*, Universitüt Zürich, Zürich, Switzerland, 1996.
53 W. Weber and W. Thiel, *Theor. Chem. Acc.*, 2000, **103**, 495.
54 A. Koslowski, M. E. Beck and W. Thiel, *J. Comput. Chem.*, 2003, **24**, 714.
55 W. Thiel, *MNDO program, version 6.1.*, Mülheim an der Ruhr, Germany, 2010.
56 M. Wanko, M. Hoffmann, P. Strodel, A. Koslowski, W. Thiel, F. Neese, T. Frauenheim and M. Elstner, *J. Phys. Chem. B*, 2005, **109**, 3606.
57 M. Hoffmann, M. Wanko, P. Strodel, P. H. Konig, T. Frauenheim, K. Schulten, W. Thiel, E. Tajkhorshid and M. Elstner, *J. Am. Chem. Soc.*, 2006, **128**, 10808.
58 M. R. Silva-Junior and W. Thiel, *J. Chem. Theory. Comput.*, 2010, **6**, 1546.
59 E. Fabiano, T. W. Keal and W. Thiel, *Chem. Phys.*, 2008, **349**, 334.
60 Z. G. Lan, E. Fabiano and W. Thiel, *ChemPhysChem*, 2009, **10**, 1225.
61 Z. G. Lan, E. Fabiano and W. Thiel, *J. Phys. Chem. B*, 2009, **113**, 3548.
62 Z. G. Lan, Y. Lu, E. Fabiano and W. Thiel, *ChemPhysChem*, 2011, **12**, 1989.
63 Y. Lu, Z. Lan and W. Thiel, *Angew. Chem., Int. Ed.*, 2011, **50**, 6864.
64 O. Weingart, Z. Lan, A. Koslowski and W. Thiel, *J. Phys. Chem. Lett.*, 2011, **2**, 1506.
65 S. R. Reddy and S. Mahapatra, *J. Chem. Phys.*, 2012, 136.
66 G. Cui, Z. Lan and W. Thiel, *J. Am. Chem. Soc.*, 2012, **134**, 1662.
67 B. R. Brooks, C. L. Brooks, III, A. D. Mackerell, Jr., L. Nilsson, R. J. Petrella, B. Roux, Y. Won, G. Archontis, C. Bartels, S. Boresch, A. Caflisch, L. Caves, Q. Cui, A. R. Dinner, M. Feig, S. Fischer, J. Gao, M. Hodoscek, W. Im, K. Kuczera, T. Lazaridis, J. Ma, V. Ovchinnikov, E. Paci, R. W. Pastor, C. B. Post, J. Z. Pu, M. Schaefer, B. Tidor, R. M. Venable, H. L. Woodcock, X. Wu, W. Yang, D. M. York and M. Karplus, *J. Comput. Chem.*, 2009, **30**, 1545.
68 M. J. Frisch, G. W. Trucks, H. B. Schlegel, G. E. Scuseria, M. A. Robb, J. R. Cheeseman, J. A. Montgomery, T. Vreven, K. N. Kudin, J. C. Burant, J. M. Millam, S. S. Iyengar, J. Tomasi, V. Barone, B. Mennucci, M. Cossi, G. Scalmani, N. Rega, G. A. Petersson, H. Nakatsuji, M. Hada, M. Ehara, K. Toyota, R. Fukuda, J. Hasegawa, M. Ishida, T. Nakajima, Y. Honda, O. Kitao, H. Nakai, M. Klene, X. Li, J. E. Knox, H. P. Hratchian, J. B. Cross, V. Bakken, C. Adamo, J. Jaramillo, R. Gomperts, R. E. Stratmann, O. Yazyev, A. J. Austin, R. Cammi, C. Pomelli, J. W. Ochterski, P. Y. Ayala, K. Morokuma, G. A. Voth, P. Salvador, J. J. Dannenberg, V. G. Zakrzewski, S. Dapprich, A. D. Daniels, M. C. Strain, O. Farkas, D. K. Malick, A. D. Rabuck, K. Raghavachari, J. B. Foresman, J. V. Ortiz, Q. Cui, A. G. Baboul, S. Clifford, J. Cioslowski, B. B. Stefanov, G. Liu, A. Liashenko, P. Piskorz, I. Komaromi, R. L. Martin,

D. J. Fox, T. Keith, M. A. Al-Laham, C. Y. Peng, A. Nanayakkara, M. Challacombe, P. M. W. Gill, B. Johnson, W. Chen, M. W. Wong, C. Gonzalez and J. A. Pople, *Gaussian 03, Revision C.02*, Gaussian Inc., Wallingford, CT, 2004.
69 S. Fischer and M. Karplus, *Chem. Phys. Lett*., 1992, **194**, 252.
70 F. Noe, F. Ille, J. C. Smith and S. Fischer, *Proteins*, 2005, **59**, 534.
71 A. N. Bondar, M. Elstner, S. Suhai, J. C. Smith and S. Fischer, *Structure*, 2004, **12**, 1281.
72 Q. Sun, S. F. Wang, H. Zhang, Z. Li, C. Pifisterer, S. Fischer, S. Nanbu and S. C. Smith, *Aust. J. Chem*., 2010, **63**, 363.
73 S. Fischer, B. Windshugel, D. Horak, K. C. Holmes and J. C. Smith, *Proc. Natl. Acad. Sci. U. S. A*., 2005, **102**, 6873.
74 M. Elstner, D. Porezag, G. Jungnickel, J. Elsner, M. Haugk, T. Frauenheim, S. Suhai and G. Seifert, *Phys. Rev. B: Condens. Matter Mater. Phys*., 1998, **58**, 7260.
75 A. D. MacKerell, D. Bashford, M. Bellott, R. L. Dunbrack, J. D. Evanseck, M. J. Field, S. Fischer, J. Gao, H. Guo, S. Ha, D. Joseph-McCarthy, L. Kuchnir, K. Kuczera, F. T. K. Lau, C. Mattos, S. Michnick, T. Ngo, D. T. Nguyen, B. Prodhom, W. E. Reiher, B. Roux, M. Schlenkrich, J. C. Smith, R. Stote, J. Straub, M. Watanabe, J. Wiorkiewicz-Kuczera, D. Yin and M. Karplus, *J. Phys. Chem. B*, 1998, **102**, 3586.
76 A. D. Becke, *J. Chem. Phys*., 1993, **98**, 5648.
77 C. Lee, W. Yang and R. G. Parr, *Phys. Rev. B: Condens. Matter Mater. Phys*., 1988, **37**, 785.
78 A. Schäfer, C. Huber and R. Ahlrichs, *J. Chem. Phys*., 1994, **100**, 5829.
79 R. Ahlrichs, M. Bär, M. Häser, H. Horn and C. Kölmel, *Chem. Phys. Lett*., 1989, **162**, 165.
80 W. Smith and T. R. Forester, *J. Mol. Graphics*, 1996, **14**, 136.
81 Chemshell a Computational Chemistry Shell, see www.chemshell.org (accessed on March 6, 2012).
82 P. Sherwood, A. H. de Vries, M. F. Guest, G. Schreckenbach, C. R. A. Catlow, S. A. French, A. A. Sokol, S. T. Bromley, W. Thiel, A. J. Turner, S. Billeter, F. Terstegen, S. Thiel, J. Kendrick, S. C. Rogers, J. Casci, M. Watson, F. King, E. Karlsen, M. Sjøvoll, A. Fahmi, A. Schäfer and C. Lennartz, *J. Mol. Struct.: THEOCHEM*, 2003, **632**, 1.
83 S. R. Billeter, A. J. Turner and W. Thiel, *Phys. Chem. Chem. Phys*., 2000, **2**, 2177.
84 T. W. Keal, A. Koslowski and W. Thiel, *Theor. Chem. Acc*., 2007, **118**, 837.
85 J. Kästner, J. M. Carr, T. W. Keal, W. Thiel, A. Wander and P. Sherwood, *J. Phys. Chem. A*, 2009, **113**, 11856.
86 T. W. Keal, M. Wanko and W. Thiel, *Theor. Chem. Acc*., 2009, **123**, 145.
87 W. Weber, V. Helms, J. A. McCammon and P. W. Langhoff, *Proc. Natl. Acad. Sci. U. S. A*., 1999, **96**, 6177.

